Micromagnetic study of flux-closure states in Fe dots using quantitative Lorentz Microscopy

Aurélien Masseboeuf, Pascale Bayle-Guillemaud, Olivier Fruchart, Fabien Cheynis, Jean-Christophe Toussaint, A. Marty

Micromagnetic study of flux-closure states in Fe dots using quantitative Lorentz Microscopy

Aurélien Masseboeuf and Pascale Bayle-Guillemaud
INAC, CEA-Grenoble - SP2M/LEMMA, 17 rue des Martyrs, Grenoble, France

Olivier Fruchart and Fabien Cheynis*
Institut NÉEL, CNRS & Université Joseph Fourier - BP166 - F-38042 Grenoble Cedex 9 - France

Jean-Christophe Toussaint
Institut NÉEL, CNRS & Université Joseph Fourier - BP166 - F-38042 Grenoble Cedex 9 - France
Grenoble INP - Grenoble, France

Alain Marty
INAC, CEA-Grenoble - SP2M/NM, 17 rue des Martyrs, Grenoble, France

A micromagnetic study of epitaxial micron-sized iron dots is reported through the analysis of Fresnel contrasts in Lorentz Microscopy. Various types of flux-closure micromagnetic states are evidenced and reconstructed using the Transport of Intensity Equation, from the simple Landau state with a single central Bloch domain wall to so-called diamond and multiple diamond states. The former was used to investigate various aspects of asymmetric Bloch domain walls. First, the experimental width of such complex walls was derived whose value and thickness-dependence was analysed with the help of numerical simulations. Moreover, quantitative datas on the magnetization inside the dot was retrieved and informations on the degrees of freedom of such walls was extracted. Finally, it is shown how the existence and the propagation of a surface vortex can be characterized and monitored. This demonstrates the ability to reach a magnetic sensitivity a priori hidden in Fresnel contrasts, based on an original image treatment and backed-up by the evaluation of contrasts obtained from micromagnetic simulations.

I. INTRODUCTION

The control of the motion of magnetic objects such as magnetic domain walls (DWs) and magnetic vortices is of great interest for their potential use in solid-state magnetic random access memories (MRAM) [3, 4]. An intense activity is currently devoted to the fundamental understanding of DW motion driven by either magnetic field or spin-polarized current, with the technological aim and fundamental need for understanding how to reach high mobilities (high speed with low field or low current).
Understanding and controlling the motion of domain-walls and vortices first requires a good knowledge of their internal micromagnetic structure. This structure is associated with one or more degrees of freedom (DoF). For instance the core of a magnetic vortex can exhibit a magnetization in an up or down state, that may be switched by a magnetic field [5] or spin-polarized currents [6]. The internal structure of vortices and DWs is best studied in dots displaying a flux-closure state, because it is stabilized in its center owing to the self dipolar field [7]. The core orientation of the magnetic vortex combined with the chirality (clockwise or anticlockwise) of the flux closure, define two DoF, that can be considered as bits in terms of data storage. Many studies have been devoted to disks with these two DoF[8–10]. Recently elongated dots with three DoF(two in the central Bloch domain wall, one in the chirality) were demonstrated, first in self-assembled dots [11] then extended to spin-valve dots [12].
Owing to its high lateral resolution and video imaging rate, Transmission Electron Microscopy (TEM - and its associated magnetic imaging technique Lorentz Microscopy - LTEM) is a powerful tool to scrutinize the inner structure of magnetic objects such as vortex arrays [13], vortices [14] or Bloch lines [15]. The resolution capacities below 10 nm [16] associated to a bulk magnetic sensivity are of great interest for such fine analysis. Furthermore, *in-situ* experiments can be carried out to monitor in real time magnetic objects such as vortices and domain walls.
It is the purpose of the present manuscript to deepen the analysis of the Lorentz microscopy investigation of flux-closure states in micron-sized self-assembled dots, both under static conditions and while monitoring the quasistatic switching of internal degrees of freedom of the DW. It is illustrated how advanced image processing of experimental data combined with post-processing of micromagnetic calculations are crucial in getting the highest possible resolution and information out of experimental data.

Section II describes the system under study and the experimental set-up. Section III is devoted to the simple

* New ad. : CINaM, CNRS-UPR3118 - F-13288 Marseille Cedex 09 - France

analysis of Fresnel contrasts used to retrieve quantitative information on the magnetic width of the DW. Section IV deals with a detailed analysis of the phase retrieval approach based on Fresnel contrasts to retrieve quantitative informations on both magnetic induction and domain wall width. New possibilities offered by high-resolution Fresnel contrast analysis are illustrated in the last section by the real-time monitoring of a magnetization process inside the DW itself, based on the propagation of a surface vortex of diameter roughly 10 nm.

II. EXPERIMENTAL SETUP

The nanostructures studied in this paper are micron-sized iron Fe(110) dots, synthesized using Pulsed-Laser Deposition under Ultra-High Vacuum conditions. The supporting surface is a 10 nm-thick W layer epitaxially-grown on 350 micron-thick Sapphire $(11\bar{2}0)$ wafers. These dots are faceted because they are single-crystalline thus displaying low Miller indices cristallographic planes. Their elongated shape is due to the uniaxial anisotropy of the (110) surface. Details about the sample growth can be found elsewhere [17]. Such dots have been extensively characterized during the past ten years by means of micromagnetic simulations [18, 19], MFM observations [18], X-ray Magnetic Circular Dichroism Photo-Emission Electron Microscopy [20] and magnetotransport [21]. The micromagnetic structure of such dots is sketched in Figure 1 and can be described as follows.
Above a lateral size of roughly 250 nm and thickness larger than 50 nm the magnetostatic energy of the dot is so large that it displays spontaneously a flux closure magnetic distribution (Fig. 1-a). Several types of flux-closure states exist in such dots [22, 23]. The simplest of these is the combination of two main domains, antiparallel one to another and oriented along the long dimension of the dot. A Bloch wall of finite length and width lies at the boundary of these two domains (Fig. 1-b). Smaller domains oriented essentially along the in-plane short axis of the dot are located at its ends, to close the flux.

The detailed inner structure of the Bloch wall is asymmetric [24, 25]. It is composed of a main out-of-plane magnetization area and two opposites so-called Néel Caps (NCs) occurring at each surface of the dot with opposite in-plane magnetization (see Fig. 1-b) [26]. At each end of the finite Bloch wall one finds a surface vortex enabling the magnetic flux to escape (in red on Fig. 1-c). These two vortices are unavoidable based on topological arguments for a flux-closure dot [27]. Thus three DoF exist in such dots: the vertical polarity of the DW, the chirality of the flux-closure and the transverse polarity of the couple of NCs (an information equivalent with the position of the two surface vortices). The controlled magnetic switching of this third DoF was demonstrated recently [11, 21].

Two microscopes were used for Lorentz Microscopy : a JEOL 3010 with a LaB_6 electron gun and a FEI Titan 80-300 kV fitted in with a Schottky gun. Both of them are working at 300kV and are fitted with a Gatan Imaging Filter for zero loss filtering [28] and thickness mapping [29]. The Titan is also equiped with a dedicated Lorentz lens for high resolution and magnetic field-free imaging while the JEOL is fitted with a conventional objective minilens initially dedicated to low magnification imaging. In-situ experiments were performed using the field produced by the objective lens of the microscope (previously calibrated using dedicated sample holders mounted with a Hall probe). A tilt of the sample was also used to produce an in-plane component of the magnetic field on the sample. Values of applied field provided here are the in-plane component of that magnetic field with respect to the given tilt angle. Samples were prepared using a mechanical polishing and ion milling. Phase retrieval using the Transport of Intensity equation [30] was thus coupled to substrate contribution removal as proposed in [31].

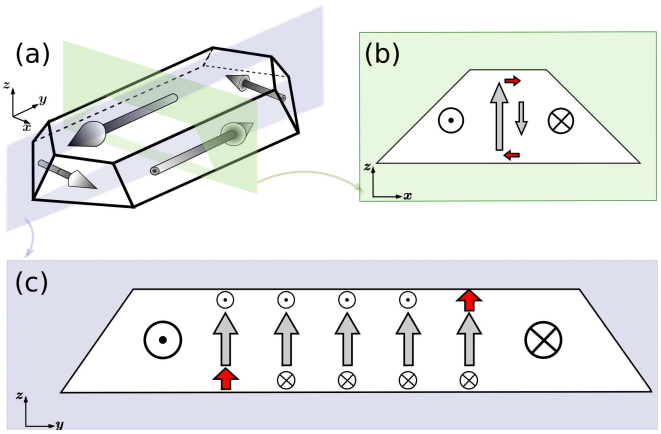

Figure 1. (Colour online) Scheme of the magnetization distribution in a single-crystalline elongated and faceted iron (110) dot. (a) Overview of the flux closure distribution in the dot. The two coloured planes are referring to the two following views. (b) Transverse section of the dot. The magnetic configuration of the asymmetric Bloch wall can be seen. The two Néel Caps are highlighted in red. (c) Longitudinal section of the dot. The overall finite Bloch wall is described here. Surface vortices are highlighted in red.

Micromagnetic simulations were performed using a custom-developed code based on a finite-differences scheme (prismatic cells) [19]. Here both a 3D and a 2D version of the code were used. The former permits the accurate description of the complex magnetic structure arising in three-dimensional structures, while the latter allows to address simple text-book cases such as an infinitely-long domain wall, and thus extract the essentials of the physics at play. We used the bulk magnetic parameters for Fe : exchange $A = 2 \times 10^{-11}$ J/m, fourth-order magnetic anisotropy $K = 4.8 \times 10^4$ J/m^3, and magnetization $M_s = 1.73 \times 10^6$ A/m.

All observations presented here are based on the Fresnel contrast [32] of LTEM. With the simple view

of geometrical optics their formation result from the overlap of two parts of the electron beam experiencing two different Lorentz forces. When an image is formed slightly over- or underfocused, this results in bright or dark lines, highlighting the domain walls. In the case of a coherent electron source, electrons should be described as waves and no more as particles, giving rise to an interference pattern at the locus of the domain wall, instead of a simple light or dark line (and are subsequently often denoted by *in-line* holography). This interference pattern contains further informations about the DW inner structure. Its detailed analysis is a chance to increase the information contained in a simple image, as it will be explained in the last section.

The sample geometry was chosen to reveal the Bloch wall contrast in Fresnel images (see Fig.3). Electron are thus travelling through the sample perpendicularly to the magnetic domains of the dot and parallely to the Bloch wall magnetization. Fig. 2 presents four different flux-closure states as color maps representing the distribution of in-plane integrated magnetic induction. These maps have been reconstructed using the phase retrieval approach of the Transport of Intensity Equation [30] linking the phase gradient in the observation plane to the intensity variation along the optical axis. This technique enables to reconstruct magnetic induction maps from Fresnel images series by estimating the derivative of the intensity with respect to the optical axis. The reconstructed phase contains an electrostatic and a magnetic component [33] that we discuss hereafter.

To retrieve quantitative magnetic information and get rid of electrostic contribution to the phase shift several techniques are available and are reviewed in [34]. The first technique we used is described in [31] and enables to remove the electrostatic contribution of the substrate to the measured phase shift for a constant gradient of substrate thickness. A value of 150±50 nm.T for the integrated magnetic induction was found where the two surfaces are parallel and the electrostatic contributions of the dot itself vanishes (i.e. far from the facets - see Fig. 2-a). Considering our experimental thickness of 70 nm (a value estimated with the log-ratio technique [29] using a value of the inelastic mean free path of 80 nm for iron at 300 kV), this value is in good agreement with the bulk iron saturated magnetization ($\mu_0 M_s = 2.17$ T). On the other hand, the possibility to reverse the chirality of the dot by an applied field [35] was used to perform a subtraction of two phase shifts with an opposite magnetic contribution. A value of 140±50 nm.T was found for the integrated magnetization in the dot. Similar procedure using a 180° reversal of the sample (realised outside the microscope) was also used and leads to the same value. These procedure was also more convenient to use as it is possible to analyse complex magnetic structures. In such a method, analysis of the diamond configuration (Fig. 2-(b)) gave the opportunity of probing the central losange quantitatively. Thickness of the dot was in this case estimated to 100 nm and a 220±50 nm.T was found for the integrated magnetization.

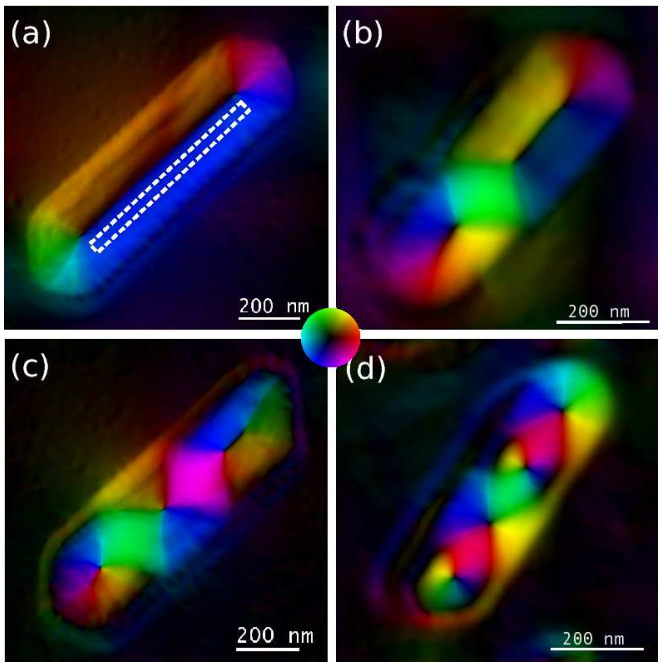

Figure 2. Four different magnetic configurations of the iron dots. **(a)** Landau state, as described in the second section. The dashed area corresponds to the location where quantitative data where extracted. **(b)** 2-Landau state where two Bloch walls, an so on, two opposite chiralities are found in the same dot. **(c)** and **(d)** 3 and 4-Landau states where most of the domain walls collapsed into a vortex state due to their limited length.

Other magnetic distributions (Fig. 2 (b-d)) can be viewed as double, triple and quadruple Landau (or also under the generic name of diamond state [18]). The number corresponds to the number of Bloch walls or vortices (if the domain wall collapses due to a too small length) inside the dot. Any of these configurations may be prepared regarding the shape of the dot and its magnetic history. Such magnetic history may be used to favor the occurrence of one or another type of state. As a general rule a saturation magnetic field (around 3T in the case of the JEOL microscope and 2T for a Titan) applied perfectly perpendicular to the dot (along z) yields a Landau state, whereas higher order states are obtained upon applying the field with a combination of an azimuthal and polar angle. Such multi-walled structure can be of fundamental use for wall length study as demonstrated in [36].

III. FRESNEL CONTRAST ANALYSIS

Fig. 3 shows three images taken for different defocus values. The 180° Bloch wall induces a bright contrast at the middle of the dot. At both extremities of this line

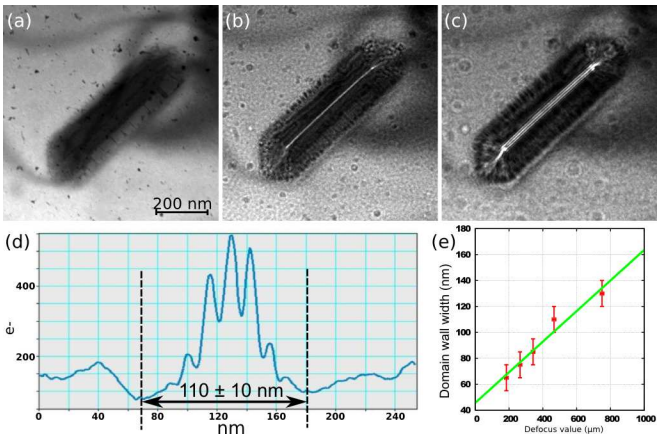

Figure 3. (a-c) Images of a Fe (110) dot for different defocus values (from (a) to (c) values of defocus are 0, 10 and 30 μm respectively). The thickness of the dot was estimated (see in the text) to 90 nm. (d) Intensity profile of the convergent wall obtained from (c) and associated width measurement (see text). (e) Zero-defocus approximation for domain wall width measurement.

weaker bright lines emerge due to Néel walls. The bright spots found at each extremity of the Bloch DW arises from the locally high curl of magnetization.
Such Fresnel contrasts can be used to assess accurately the width of the Bloch wall. We used the zero-defocus approximation that consists of a linear regression for a focal series of domain wall contrast width measurement [37]. This old fashionned [38] method has been widely used and commented. We rely here on the validity of the method regarding the large width [39] and asymetry [40] of the domain walls studied here. In that method, the width of the convergent wall is estimated by taking the width of the interference pattern, namely the distance between the two extreme bright fringes (see Fig. 3-d). We found a width for the Bloch wall of 45±5 nm.

To analyse quantitatively such value, we used our 2D micromagnetic code considering infinitely long (in the y direction) iron (110) bars with a thickness over width ratio of 0.2 which is a typical experimental value. Due firstly to the four-fold magnetocrystalline anisotropy, and secondly to the three-dimensional nature of the system, the domain wall width cannot be easily defined by a tangent like in the text-book case [41]. Choosing the most suitable definition of a DW width is mandatory for the analysis of both experiments and simulations. We used the formula described e.g. by Hubert [42] integrating over the θ angle corresponding to the magnetization orientation with respect to the wall direction (y) (both magnetization variations along x and z are described in Fig. 4 a-b):

$$\delta_w = \int_0^\infty \sin\theta_x dx \qquad (1)$$

This formula can be integrated over the thickness of

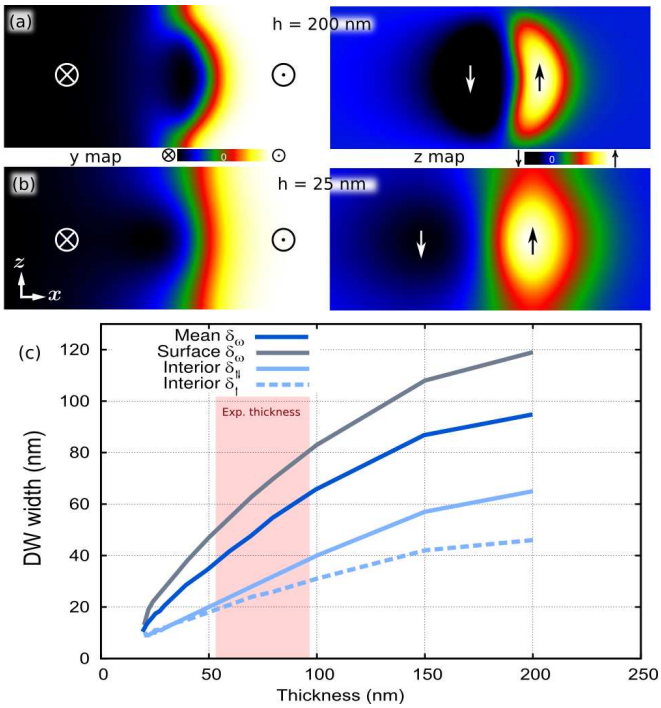

Figure 4. Domain wall width measure with respect to the thickness on simulated iron bar. **(a)** y- and z-components of the magnetization on a wall profile for a 200 nm-thick iron bar. **(b)** Same as in (a) for a 25 nm-thick iron bar with same aspect ratio. **(c)** Plot of the wall width versus thickness using various description of the domain wall width (see text). Experimental thicknesses area is reported on the graph.

the dot (*i.e.* along the z direction), or applied at any height, the surface and middle-height being of particular interest. Fig. 4-c presents resulting values of width measurements considering various descriptions given hereafter. Several comments can be made on these results.

In the low thickness regime, for any definition the DW width fits roughly linearly with the thickness. In that case one often uses the name of *vortex wall* for the obvious reason of curling of magnetization in the (x,z) plane (Fig. 4-b). The linearity results from the fact that the DW is directly constrained by the thickness of the film, and the DW profile changes homothetically with film thickness.
The DW width seems hardly to saturate for large thickness, whereas for 200 nm a steady value was nearly reached by Rave and Hubert [43]. This probably results from the fact that they used a much larger uniaxial anisotropy value than the one in Fe, yielding narrower domain walls. This steady width is much smaller than 200 nm in their case, so that bulk properties are already reached. In our case the bulk wall width is larger and the DW is still geometrically constrained at 200 nm thickness and ever more below (Fig. 4-a).
Aside the DW, we observe an area with a weak verti-

cal component of magnetization of sign opposite to that of the core of the DW (see z-maps on Fig. 4-a and b). Whereas this was already visible in the early simulations of Hubert [24] and LaBonte [25], this feature is nearly absent in the extensive calculations reported more recently because again of the choice of a high value of anisotropy, inducing the magnetization to remain in-plane as much as possible [44, 45]. The presence of this component implies a more careful description of how the domain wall width should be defined : with or without taking into account this extra inner feature. Two distinct approaches can be used considering ($\delta_{\uparrow\downarrow}$) or not ($\delta_{\uparrow}$) this opposite component of the wall (i.e. when $m_z \leqslant 0$, see also Fig. 1-b). As an illustration, Fig. 4 shows the mean DW width computed from Eq. 1 and integrated over the thickness for both cases. The results show large differences with the full integral calculation showing that care should be taken when discussing the width of such walls.
Experimentally it is found that for a thickness of 70 nm the width is $\delta = 45$ nm. This value fits better with the mean δ_w definition which is coherent with the integration along the electron path which is made when using Lorentz microscopy. Therefore such a description is the most inappropriate way to describe the width of complex asymetric Bloch DWs. Nevertheless this measurement gives useful information on the wall profile as the inner widths can be estimated with respect to the average value. We will see in the last part of that study how it is possible to analyse carefully Fresnel contrasts to obtain more spatial information on the magnetization distribution in such walls.

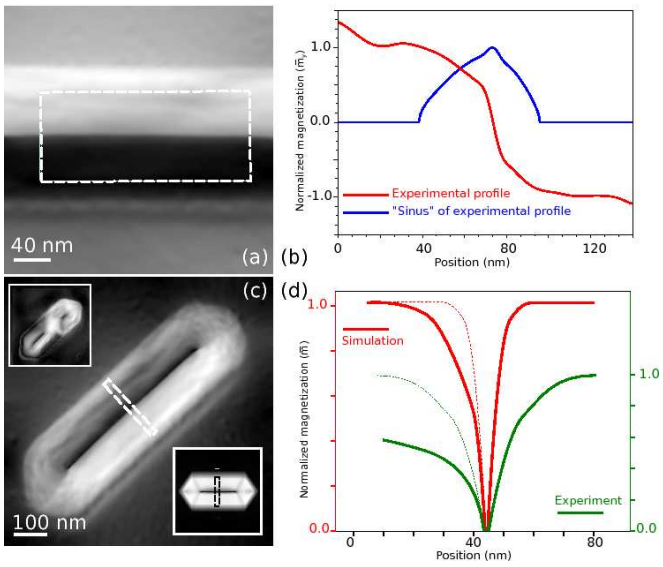

Figure 5. TIE reconstruction analysis. (a) Experimental phase gradient along x representing the y component of the integrated magnetization. (b) Experimental profile taken in (a) and its associated "positive sinus" approximation (see text). (c) Experimental modulus of the integrated induction calculated using two perpendicular phase gradients. Inset on the top-left is the same display on another dot displaying a double Landau configuration. The bottom-right inset is a simulated integrated induction map from micromagnetic modeling. The dashed lines show localisation of profiles presented in (d). (d) Profiles extracted from (c). The continous lines display the extracted profiles of the integrated magnetic induction maps for the simulated and experimental maps. Dashed lines show what would be expect for a symetric wall.

IV. PHASE-SHIFT ANALYSIS

As the phase-shift retrieval is based on a defocused measurement we do not expect to get a better resolution in measuring the domain wall width by such a method. However a phase shift is often regarded as containing more information than a simple Fresnel image. We performed measurements of the wall width based on the phase shift gradient as described in Fig. 5 (a-b). The gradient is there used as an approximation of the cosinus of the wall angle, the values of the integrated magnetization being normalized between +1 and -1. The sinus used in the description by Hubert (Eq. 1) was thus estimated by taking the real part of $\sqrt{1-\bar{m}_y{}^2}$, $\bar{m}_y$ being the integrated magnetization along wall direction. Such a description helps in avoiding experimental fluctuations around the maximum value of $\bar{m}_y$. Integration leads to a value of 54 ± 10 nm which fits with the zero-defocus estimation. The over-estimation is explained by the use of an out-of-focus method and could be linked to the value of the defocalisation used in the reconstruction.
Moreover, a full map of $\bar{m} = \sqrt{\bar{m}_x{}^2 - \bar{m}_y{}^2}$ gives further informations that cannot be reach in simple Fresnel contrasts. As it is shown in Fig. 5 (c-d) the $\bar{m}$ map derived from two prependicular phase gradients contains a useful information on the third DoF described above. As such a DoF is carried by the chirality of the asymetric Bloch wall, the integrated $\bar{m}$ exhibits a decrease in value around the Bloch wall location. The two NCs are perfectly antiparallel and give no signal in $\bar{m}$. On the contrary, the presence of a small amount of perpendicular magnetization between these two NCs (see Fig. 1-(b)) leads to a local decrease of $\bar{m}$. In both experimental (Fig. 5-(c)) and simulated (bottom right inset on same figure) case, one can see an asymetry in the wall profile made on the $\bar{m}$ map (Fig. 5-(d)). This asymetry on one side or the other of the domain wall location gives a unambigous information on the position of the anti-parallel part of the asymetric Bloch wall thus leading to the chirality information. Such a description can also be made when several walls are standing in the dot : top-left inset of Fig. 5 (c) shows a double-Landau configuration where the two Bloch DWs exhibit two opposite chiralities. A combination of such analysis with a study of the wall polarity as it was recently proposed in [46] could lead to a full description of the three DoF in such structures.

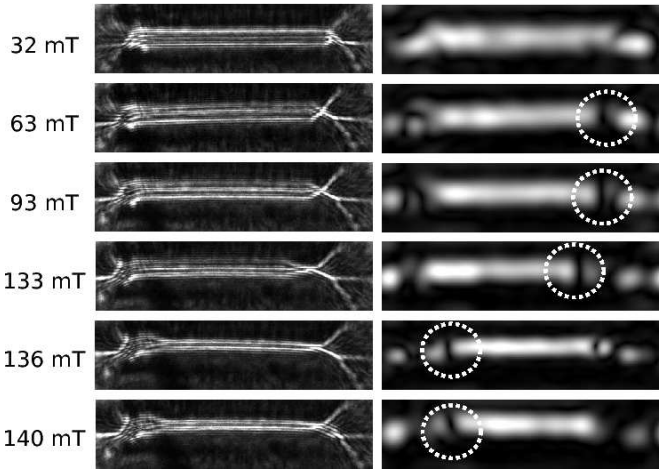

Figure 6. Experimental Fresnel contrasts (left column) and associated amplitude (right column) analysis for corresponding fringe frequency. The corresponding in-plane component of the applied magnetic field is indicated in the first column for each row.

V. FRESNEL CONTRAST EXPLORATION

From a general point of view LTEM suffers from a limited sensitivity because an integration is made over all the electron path. Here we demonstrate how the induced fringes of a convergent wall can be analysed to yield highly-resolved information about the domain walls. A comparison with micromagnetic modelling and contrast simulation is also given to confirm our observations.

We focus on the process of reversal of Néel caps, mediated by the motion of a surface vortex along the length of the domain wall. One can find detailed information on the process in [11, 21]. One considers in that section that the surface vortex is a simple perturbation of the Bloch wall. Its displacement along the Bloch wall only slightly modifies the local magnetization distribution. When increasing the defocus of the imaging lens, the overlap of the electrons coming from the neighbouring domains becomes wider and as a result the number of interference fringes increases. If the defocus is high enough (namely close to a millimetre) the interference pattern created can be compared to a small off-axis hologram [47], bearing a wealth of information. Inner details of the DW can then be derived from the analysis of these fringes, such as the location of a surface vortex. The result is shown in Fig. 6.

Both original and amplitude images of the fringes are presented. The amplitude image corresponds to a wave reconstructed with the spatial frequency of the fringes and thus displays the location of the fringes in the image. The first image taken at 32 mT is the starting point of the series with the vortex located to the right side. On the following images the fringe perturbation created by the vortex displacement can be seen with the straight dark

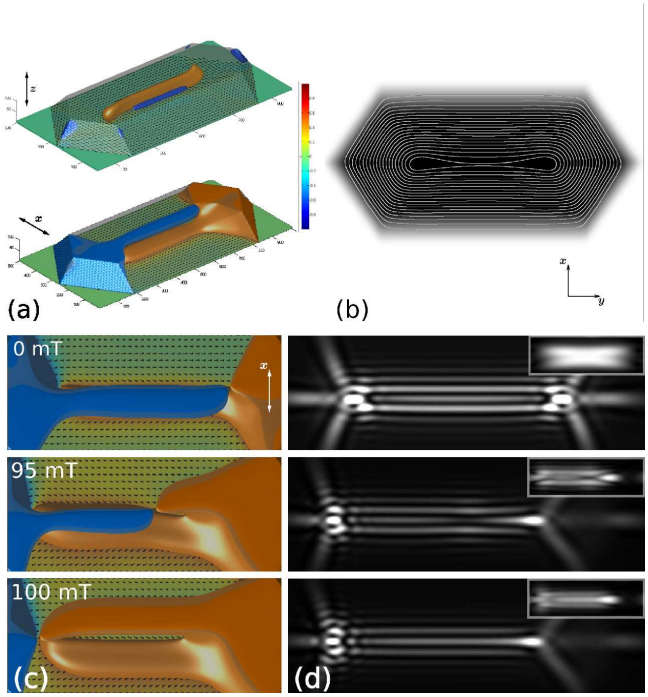

Figure 7. Three dimensional micromagnetic modelling of the iron dots during a transverse magnetic field application and associated computed Fresnel contrasts. **(a)** The z and x components of the magnetization displayed in two different drawings. Both are represented with a minimum threshold of $\pm M_s/2$ to provide us with an easily readable open-view of the dot. **(b)** Phase shift associated to the micromagnetic modelling at zero degree tilt. **(c)** Three different modellings (x-component displayed as in (a)) for various transverse applied fields. **(d)** Associated Fresnel contrast simulation for a defocus of 750 μm.

line in the amplitude image (highlighted with dashed circles on Fig. 6) indicating that the fringes are locally suppressed. The vortex is moving from the right extremity (at 63, 93 and 133 mT) along the domain wall and reaches its other extremity. The final transition occurs here between 133 and 136 mT. After this transition, the perturbation disappears and the wall exhibits a contrast similar to that observed on original images. The phenomenon is hysteretic and on the decreasing field series the magnetic switching happens between 123 and 121 mT.

A code to simulate Fresnel contrasts from three-dimensional micromagnetic simulations was developed. The tilt of the sample used for in-plane field application is modelled using a barycentre approach : each three-dimensional voxel of the micromagnetic simulation is projected onto a plane. If the projected voxel is misaligned with the new mesh of the magnetic distribution, its value is spread on the four nearest neighbours depending on its center of mass in this square. The determined phase shift is also associated with a simple object plane without a thickness. Note that the defocus used experimentally and in simulation is very important (close to mm) regarding the thickness of the dot (100 nm). The assumption of

a simple phase object with no thickness should thus be valid.

Fig. 7-a and b present the three-dimensional modelling and its associated phase-shift. As stated above, a simple analysis of the phase shift gives no information on the loci of the surface vortices. Simulated Fresnel contrasts obtained from simulation with various transverse applied fields (Fig. 7-c and d) yield a similar perturbation that on experimental Fresnel fringes. Analysis of simulated contrats as it was proceed on experimental images (see amplitudes images as inset on Fig. 7-(d)) did not show as much contrast because of the low sampling use in simulations. It is here obvious that the propagation of the surface vortex can be analysed by such a perturbation in the Fresnel fringes.

VI. CONCLUSION

We have described the micromagnetic configuration of epitaxially grown (110) iron dots. The micromagnetic knowledge of these dots has been retrieved by Lorentz microscopy observations. These observations enabled to measure the domain wall width of an asymmetric Bloch wall, and to compare it successfully with micromagnetic simulations. It also allowed to define more clearly how such asymetric wall may be defined in terms of width measurement. Two of the 3 dergrees of freedom in such structure where also determined. Besides, various magnetic configurations were highlighted during phase retrieval processes. All these configurations could be easily obtained by modifying the magnetic history of the dots. Finally, the switching process of the Néel Caps surrounding the central Bloch wall was perfectly described with the used of interference patterns created in Fresnel contrasts, underlining the potential of high-coherence microscopes in getting the highest resolution information using Lorentz microscopy.

[1]

[2] 08, 1.

[3] D. A. Allwood, G. Xiong, C. C. Faulkner, D. Atkinsion, D. Petit, and R. P. Cowburn. Magnetic domain-wall logic. Science, 309:1688, 2005.

[4] S. S. P. Parkin, M. Hayashi, and L. Thomas. Magnetic domain-wall racetrack memory. Science, 320(5873):190–194, Apr 2008.

[5] K. Yamada, S. Kasai, Y. Nakatani, K. Kobayashi, H. Kohno, A. Thiaville, and T. Ono. Electrical switching of the vortex core in a magnetic disk. Nature Materials, 6(4):269–263, Apr 2007.

[6] B. Van Waeyenberge, A. Puzic, H. Stoll, K. W. Chou, T. Tyliszczak, R. Hertel, M. Fahnle, H. Bruckl, K. Rott, G. Reiss, I. Neudecker, D. Weiss, C. H. Back, and G. Schutz. Magnetic vortex core reversal by excitation with short bursts of an alternating field. Nature, 444(7118):461–464, November 2006.

[7] M. Schneider, H. Hoffmann, S. Otto, Th. Haug, and J. Zweck. Stability of magnetic vortices in flat submicron permalloy cylindes. Journal of Applied Physics, 92:1466–1472, 2002.

[8] M. Schneider, H. Hoffmann, and J. Zweck. Magnetic switching of single vortex permalloy elements. Applied Physics Letters, 79(19):3113, 2001.

[9] T. Kimura, Y. Otani, and J. Hamrle. Determination of magnetic vortex chirality using lateral spin-valve geometry. Applied Physics Letters, 87(17):172506, 2005.

[10] Z. Zhong, H. Zhang, X. Tang, Y. Jing, L. Jia, and S. Liu. Vortex chirality control in magnetic submicron dots with asymmetrical magnetic properties in lateral direction. Journal of Magnetism and Magnetic Materials, 321(15):2345–2349, August 2009.

[11] F. Cheynis, A. Masseboeuf, O. Fruchart, N. Rougemaille, J. C. Toussaint, R. Belkhou, P. Bayle-Guillemaud, and A. Marty. Controlled switching of neel caps in flux-closure magnetic dots. Physical Review Letters, 102(10):107201, 2009.

[12] L. Huang and Y. Zhu. Controlled reversal of coupled nel walls in flux-closure magnetic trilayer elements. Applied Physics Letters, 95(22):222502, 2009.

[13] A. Tonomura, H. Kasai, O. Kamimura, T. Matsuda, K. Harada, T. Yoshida, T. Akashi, J. Shimoyama, K. Kishio, T. Hanaguri, K. Kitazawa, T. Masui, S. Tajima, N. Koshizuka, P. L. Gammel, D. Bishop, M. Sasase, and S. Okayasu. Observation of structures of chain vortices inside anisotropic high-t-c superconductors. PHYSICAL REVIEW LETTERS, 88:237001, June 2002.

[14] M. Beleggia, G. Pozzi, J. Masuko, N. Osakabe, K. Harada, T. Yoshida, O. Kamimura, H. Kasai, T. Matsuda, and A. Tonomura. Interpretation of lorentz microscopy observations of vortices in high-temperature superconductors with columnar defects. Physical Review B, 66(17):174518, November 2002.

[15] A. Masseboeuf, T. Jourdan, F. Lancon, P. Bayle-Guillemaud, and A. Marty. Probing magnetic singularities during magnetization process in FePd films. Applied Physics Letters, 95(21):212501–3, November 2009.

[16] Mihaela Tanase and Amanda K. Petford-Long. In situ tem observation of magnetic materials. Microscopy Research and Technique, 72(3):187–196, 2009.

[17] O. Fruchart, P.O. Jubert, M. Eleoui, F. Cheynis, B. Borca, P. David, V. Santonacci, A. Lienard, M. Hasegawa, and C. Meyer. Growth modes of fe(110) revisited : a contribution of self-assembly to magnetic materials. J. Phys. : Condens. Matter, 19:053001, 2007.

[18] P.O. Jubert, J.C. Toussaint, O. Fruchart, C. Meyer, and Y. Samson. Flux-closure-domain states and demagnetizing energy determination in sub-micron size magnetic dots. Europhysics Letters, 63:135–141, 2003.

[19] O. Fruchart, J. C. Toussaint, P. O. Jubert, W. Wernsdorfer, R. Hertel, J. Kirschner, and D. Mailly. Angular-dependence of magnetization switching for a multi-domain dot: experiment and simulation,. Physical Review B, 70:172409–1–4, 2004.

[20] R. Hertel, O. Fruchart, S. Cherifi, P. O. Jubert, S. Heun, A. Locatelli, and J. Kirschner. Three-dimensional magnetic flux-closure patterns in mesoscopic fe islands. Physical Review B, 72:214409, 2005.

[21] F. Cheynis, H. Haas, T. Fournier, L. Ranno, W. Wernsdorfer, O. Fruchart, and J.-C. Toussaint. Contacting individual fe(110) dots in a single electron-beam lithography step. Nanotechnology, 20:285302, 2009.

[22] R. Hertel and H. Kronmüller. Computation of the magnetic domain structure in bulk permalloy. Phys. Rev. B, 60:7366–7378, 1999.

[23] M. Bode, A. Wachowiak, J. Wiebe, A. Kubetzka, M. Morgenstern, and R. Wiesendanger. Thickness dependent magnetization states of fe islands on w(110): from single domain to vortex and diamond patterns. Applied Physics Letters, 84:948, 2004.

[24] A. Hubert. Stray-field-free magnetization configurations. Physica Statuts Solidi, 32:519, 1969.

[25] A. E. LaBonte. Two-dimensional bloch-type domain walls in ferromagnetic films. Journal of Applied Physics, 40(6):2450, 1969.

[26] S. Foss, R. Proksh, D. Dahlberg, B. Moskowitz, and B. Walsch. Localized micromagnetic perturbation of domain walls in magnetite using a magnetic force microscope. Applied Physics Letters, 69:3426, 1996.

[27] A. Arrott, B. Heinrich, and A. Aharoni. Point singularities and magnetization reversal in ideally soft ferromagnetic cylinders. IEEE Trans. Magn., 15:1228, 1979.

[28] J. Dooley and M. De Graef. Energy filtered magnetic induction mapping. Micron, 28(5):371–380, October 1997.

[29] T. Malis, S. C. Cheng, and R. F. Egerton. Eels log-ratio technique for specimen-thickness measurement in the tem. J Electron Microsc Tech, 8(2):193–200, Feb 1988.

[30] D. Paganin and K.A. Nugent. Noninterferometric phase imaging with partially coherent light. Physical review letters, 80:2586–2589, 1998.

[31] A. Masseboeuf, C. Gatel, P. Bayle-Guillemaud, A. Marty, and J-C. Toussaint. Lorentz microscopy mapping for domain wall structure study in l1(0) fepd thin films. Ultramicroscopy, 110(1):20–5, 2009.

[32] J.N. Chapman. The investigation of magnetic domain structures in thin foils by electron microscopy. Journal of Physics D : Applied Physics, 17:623–647, 1984.

[33] Y. Aharonov and D. Bohm. Significance of electromagnetic potentials in the quantum theory. Physical Review, 115(3):485–491, 1959.

[34] R. E. Dunin-Borkowski, T. Kasama, A. Wei, S. L. Tripp, M. J. Hytch, E. Snoeck, R. J. Harrison, and A. Putnis. Off-axis electron holography of magnetic nanowires and chains, rings, and planar arrays of magnetic nanoparticles. Microscopy Research And Technique, 64(5-6):390–402, August 2004.

[35] A. Masseboeuf, N. Rougemaille, J.C. Toussaint, P. Bayle-Guillemaud, and O. Fruchart. In preparation.

[36] A. Masseboeuf, O. Fruchart, J. C. Toussaint, E. Kritsikis, L. Buda-Prejbeanu, F. Cheynis, P. Bayle-Guillemaud, and A. Marty. Dimensionality crossover in magnetism: From domain walls (2D) to vortices (1D). Physical Review Letters, 104(12):127204, March 2010.

[37] S. J. Lloyd, J. C. Loudon, and P. A. Midgley. Measurement of magnetic domain wall width using energy-filtered fresnel images. Journal of Microscopy-oxford, 207:118–128, 2002.

[38] D. H. Warrington. An investigation into the use of intensity observations in the electron microscope for determining magnetic domain wall widths in thin foils. Philosophical Magazine, 9(98):261–275, 1964.

[39] H. Gong and J. N. Chapman. On the use of divergent wall images in the fresnel mode of lorentz microscopy for the measurement of the widths of very narrow domain walls. Journal of Magnetism and Magnetic Materials, 67(1):4–8, May 1987.

[40] J. Marti and W. F. Lewis. The validity of the extrapolation technique for measuring wall widths in asymmetric domain walls. Journal of Applied Physics, 48(7):3167–3168, 1977.

[41] F. Bloch. Zur theorie des austauschproblems und der remanenzerscheinung der ferromagnetika. Zeitschrift fr Physik A Hadrons and Nuclei, 74:295, 1932.

[42] A. Hubert and R. Shfer. Magnetic Domains. Springer, 1998.

[43] W. Rave and A. Hubert. Micromagnetic calculation of the thickness dependence of surface and interior width of asymmetrical bloch walls. Journal of Magnetism and Magnetic Materials, 184(2):179–183, April 1998.

[44] L. Korzunin, B. Filippov, F. Kassan-Ogly, and I. Chaĭkovsky. Static properties of asymmetric vortex-like domain walls in magnetically uniaxial thick films. Physics of the Solid State, 48(9):1732–1737, 2006.

[45] L. G. Korzunin, B. N. Filippov, and F. A. Kassan-Ogly. New types of asymmetric domain walls in magnetically triaxial films with a (100) surface. The Physics of Metals and Metallography, 109(1):15–21, 2010.

[46] Duc-The Ngo and Stephen McVitie. Visualization of vortex core polarity in nife nanodots by tilted fresnel images. Ultramicroscopy, In Press, 2011.

[47] J.M. Cowley. Twenty form of electron holography. Ultramicroscopy, 41:335–348, 1992.